

# On shape coexistence and possible shape isomers of nuclei around $^{172}\text{Hg}^*$

Xin Guan,<sup>1,†</sup> Jing Guo,<sup>1</sup> Qi-Wen Sun,<sup>1</sup> Bożena Nerlo-Pomorska,<sup>2</sup> and Krzysztof Pomorski<sup>3</sup>

<sup>1</sup>*School of Physics and Electronic Technology, Liaoning Normal University, Dalian 116029, China*

<sup>2</sup>*Institute of Physics, Maria Curie Skłodowska University, 20-031 Lublin, Poland*

<sup>3</sup>*National Centre for Nuclear Research, 02-093 Warsaw, Poland*

This study explores the phenomenon of shape coexistence in nuclei around  $^{172}\text{Hg}$ , with a focus on the isotopes  $^{170}\text{Pt}$ ,  $^{172}\text{Hg}$ , and  $^{174}\text{Pb}$ , as well as the  $^{170}\text{Pt}$  to  $^{180}\text{Pt}$  isotopic chain. Utilizing a macro-microscopic approach that incorporates the Lublin-Strasbourg Drop model combined with a Yukawa-Folded potential and pairing corrections, we analyze the potential energy surfaces (PESs) to understand the impact of pairing interaction.

For  $^{170}\text{Pt}$ , the PES exhibited a prolate ground-state, with additional triaxial and oblate-shaped isomers. In  $^{172}\text{Hg}$ , the ground-state deformation transitions from triaxial to oblate with increasing pairing interaction, demonstrating its nearly  $\gamma$ -unstable nature. Three shape isomers (prolate, triaxial, and oblate) were observed, with increased pairing strength leading to the disappearance of the triaxial isomer.  $^{174}\text{Pb}$  exhibited a prolate ground-state that became increasingly spherical with stronger pairing. While shape isomers were present at lower pairing strengths, robust shape coexistence was not observed. For realistic pairing interaction, the ground-state shapes transitioned from prolate in  $^{170}\text{Pt}$  to a coexistence of  $\gamma$ -unstable and oblate shapes in  $^{172}\text{Hg}$ , ultimately approaching spherical symmetry in  $^{174}\text{Pb}$ . A comparison between Exact and Bardeen-Cooper-Schrieffer (BCS) pairing demonstrated that BCS pairing tends to smooth out shape coexistence and reduce the depth of the shape isomer, leading to less pronounced deformation features.

The PESs for even-even  $^{170-180}\text{Pt}$  isotopes revealed significant shape evolution.  $^{170}\text{Pt}$  showed a prolate ground-state, whereas  $^{172}\text{Pt}$  exhibited both triaxial and prolate shape coexistence. In  $^{174}\text{Pt}$ , the ground-state was triaxial, coexisted with a prolate minimum. For  $^{176}\text{Pt}$ , a  $\gamma$ -unstable ground-state coexists with a prolate minimum. By  $^{178}\text{Pt}$  and  $^{180}\text{Pt}$ , a dominant prolate minimum emerged. These results highlight the role of shape coexistence and  $\gamma$ -instability in the evolution of nuclear structure, especially in the mid-shell region.

These findings highlight the importance of pairing interactions in nuclear deformation and shape coexistence, providing insights into the structural evolution of mid-shell nuclei.

Keywords: Macro-micro model, Shape coexistence, Shape isomers, Exact and BCS pairing solutions

## I. INTRODUCTION

Shape coexistence in atomic nuclei has garnered significant attention in the field of nuclear physics and has become a prominent topic in contemporary research. This phenomenon refers to the presence of multiple distinct shapes within a single nucleus, where states with similar energies exhibit different deformations [1]. Understanding nuclear shapes is crucial for revealing the internal structure and properties of nuclei, providing tools for predicting and explaining nuclear behaviors, and advancing nuclear physics [2–6].

The study of nuclear shapes has a long history, with several foundational studies laying the groundwork for our current understanding. Early theoretical developments included Rainwater's 1950 paper [7], which first proposed the idea of nuclear deformation, and Bohr and Mottelson's collective model [8, 9], which provided a framework for describing rotational spectra in deformed nuclei. Arima and Horie's 1954 study [10] explored the role of configuration mixing in nuclear structure, while Nilsson's work [11] introduced a shell-model approach incorporating deformation effects. Around the same time, Morinaga's 1956 paper [12] specifically addressed the structure of  $^{16}\text{O}$  and explained the properties of its first excited state and ground state. He introduced the concept

of multi-nucleon cross-shell excitation to describe the deformation characteristics, offering a new perspective on how nuclear shapes evolve. Further developments include Elliott's work in 1958 [13], which further developed the concept of SU(3) symmetry in nuclear deformation and highlighted the interplay between single-particle and collective motion. Over the past five decades, shape coexistence has evolved from a rare phenomenon to a common feature observed in many nuclei, highlighting its significance in nuclear structure research [14]. Recent experimental studies have revealed significant evidence of shape coexistence phenomena in neutron-deficient isotopes of lead and mercury. For instance, one study [15] specifically focuses on the  $^{188}\text{Hg}$  isotope, where theoretical predictions suggest the presence of shape coexistence.

These findings have led to increased theoretical investigations into nuclear shape coexistence, utilizing advanced experimental techniques such as tagging techniques at the University of Jyväskylä, Coulomb-excitation experiments at CERN, and relativistic energy-fragmentation experiments at GSI [16]. These experiments underscore the importance of understanding the mechanisms governing the evolution of nuclear shape. Building upon these experimental insights, theoretical investigations have played a pivotal role in elucidating the complexities of shape coexistence [17–19]. Previous studies have employed various theoretical frameworks, including macro-microscopic approaches and self-consistent models, to perform comprehensive calculations of nuclear ground-state masses and deformations across a wide range of nuclei [14].

\* Supported by the National Natural Science Foundation of China (No.12275115,12175097).

† Corresponding author, [Xin Guan, guanxin@lnnu.edu.cn](mailto:Xin Guan, guanxin@lnnu.edu.cn).

Ref. [20] highlighted the presence of two distinct coexisting configurations, in platinum isotopes  $^{176-186}\text{Pt}$ , oblate and prolate, revealing the intricate shape evolution in this mass region. Therefore, shape coexistence in even-even  $^{172-200}\text{Hg}$  isotopes was comprehensively studied using the interacting boson model with configuration mixing [21]. Recently, using the Lublin-Strasbourg Drop (LSD) with Yukawa-Folded single-particle potential and the BCS pairing correction in a macro-microscopic model, Pomorski et al. provided the deformation PESs of nuclei near  $Z = 82$ . Their study investigated the shape coexistence phenomenon in even-even isotopes of Pt, Hg, and Pb [22]. These studies revealed that nuclei in the vicinity of Hg exhibit a rich variety of shape coexistence phenomena, characterized by the interplay of spherical, oblate, and prolate configurations. Although significant progress has been made in understanding these features of heavier isotopes, lighter isotopes of Hg, Pt, and Pb have been relatively underexplored owing to the scarcity of experimental data [23]. To address this gap, further theoretical investigations are crucial, as they can illuminate the evolution of shape coexistence in these lighter isotopes. Such efforts would not only enhance our theoretical understanding but also provide valuable guidance for future experimental measurements, enabling better interpretation of the limited or ambiguous data that are currently available.

Despite its success, the BCS method [24], as well as the more refined Hartree-Fock-Bogolyubov (HFB) approach face limitations due to the small number of valence nucleons under the pairing correlation's influence [25–31]. These methods often fail to conserve particle numbers, leading to inaccuracies in describing higher-lying excited states [32]. Alternatives such as the shell model provide successful descriptions but are limited by the combinatorial growth of model space sizes, necessitating truncation schemes for heavy nuclei and often being constrained by computational resources [33]. Recent advancements in shell-model truncation techniques, such as the Monte Carlo shell model [34] and angular momentum-projected number-conserved BCS approach [35], have made significant progress in describing deformed nuclei in heavy mass regions, offering improved computational feasibility while maintaining accuracy.

The Exact solution to the standard pairing problem, first obtained by Richardson and now referred to as the Richardson-Gaudin method, offers a promising approach for the microscopic treatment of clustering in heavy nuclei [36–39]. This method is particularly suitable for handling the large model spaces and the pairing and shell effects necessary for accurately describing heavy nuclei [40–43]. In our previous work, the deformed mean-field plus pairing model within the Richardson-Gaudin method was used to explore the quantum phase transition around neutron number  $N \approx 90$  in the  $A \approx 150$  mass region [44]. The analysis demonstrated the critical behavior of the shape phase transition driven by competition between deformation and pairing interactions. More recently, a new iterative algorithm was developed to find the Exact solution to the standard pairing problem within the Richardson-Gaudin method [45], which has shown excellent agreement with experimental data when applied to actinide

fission nuclei isotopes [46–48].

The aim of the current study is to extend this line of inquiry by presenting a systematic study of PESs for even-even Pt, Hg, and Pb isotopes near  $Z = 82$ . Our investigation leverages recent advancements in shape parametrization and adopted a macro-microscopic approach, integrating the LSD model with a Yukawa-Folded single-particle potential. The analysis focuses on the impact of pairing interactions on the shape coexistence of  $^{170}\text{Pt}$ ,  $^{172}\text{Hg}$ ,  $^{174}\text{Pb}$  nuclei, as well as  $^{170-180}\text{Pt}$  even-even isotopes.

## II. THEORETICAL FRAMEWORK AND NUMERICAL DETAILS

### A. Deformed mean-field plus standard pairing model

The Hamiltonian of the deformed mean-field plus standard pairing model for either the proton or the neutron sector is given by

$$\hat{H} = \sum_{i=1}^n \varepsilon_i \hat{n}_i - G \sum_{ii'} S_i^+ S_{i'}^-, \quad (1)$$

where the sums run over all given  $i$ -double degeneracy levels of total number  $n$ ,  $G > 0$  is the overall pairing interaction strength,  $\{\varepsilon_i\}$  are the single-particle energies obtained from mean-field, such as Hartree-Fock, Woods-Saxon potential, Yukawa-Folded single-particle potential, or Nilsson model.  $n_i = a_{i\uparrow}^\dagger a_{i\uparrow} + a_{i\downarrow}^\dagger a_{i\downarrow}$  is the fermion number operator for the  $i$ -th double degeneracy level, and  $S_i^+ = a_{i\uparrow}^\dagger a_{i\downarrow}^\dagger$ ,  $[S_i^- = (S_i^+)^\dagger = a_{i\downarrow} a_{i\uparrow}]$  is the pair creation (annihilation) operator. The up and down arrows in these expressions refer to time-reversed states.

According to the Richardson-Gaudin method [36–39], the exact  $k$ -pair eigenstates of (1) with  $\nu_{i'} = 0$  for even systems or  $\nu_{i'} = 1$  for odd systems, in which  $i'$  is the label of the double degeneracy level that is occupied by an unpaired single particle can be written as

$$|k; \xi; \nu_{i'}\rangle = S^+(x_1^{(\xi)}) S^+(x_2^{(\xi)}) \cdots S^+(x_k^{(\xi)}) |\nu_{i'}\rangle, \quad (2)$$

where  $|\nu_{i'}\rangle$  is the pairing vacuum state with the seniority  $\nu_{i'}$  that satisfies  $S_i^- |\nu_{i'}\rangle = 0$ , and  $\hat{n}_i |\nu_{i'}\rangle = \delta_{ii'} \nu_{i'} |\nu_{i'}\rangle$  for all  $i$ . Here,  $\xi$  is an additional quantum number for distinguishing different eigenvectors with the same quantum number  $k$  and

$$S^+(x_\mu^{(\xi)}) = \sum_{i=1}^n \frac{1}{x_\mu^{(\xi)} - 2\varepsilon_i} S_i^+, \quad (3)$$

in which the spectral parameters  $x_\mu^{(\xi)}$  ( $\mu = 1, 2, \dots, k$ ) satisfy the following set of Bethe ansatz equations (BAEs):

$$1 + G \sum_i \frac{\Omega_i}{x_\mu^{(\xi)} - 2\varepsilon_i} - 2G \sum_{\mu'=1(\neq\mu)}^k \frac{1}{x_\mu^{(\xi)} - x_{\mu'}^{(\xi)}} = 0, \quad (4)$$

where the first sum runs over all  $i$  levels and  $\Omega_i = 1 - \delta_{ii'}\nu_{i'}$ .  
For each solution, the corresponding eigenenergy is given by

$$E_k^{(\xi)} = \sum_{\mu=1}^k x_{\mu}^{(\xi)} + \nu_{i'}\varepsilon_{i'}. \quad (5)$$

In general, according to the polynomial approach in Refs. [41–43], one can find solutions of Eq. (4) by solving the second-order Fuchsian equation [40] as

$$A(x)P''(x) + B(x)P'(x) - V(x)P(x) = 0, \quad (6)$$

where  $A(x) = \prod_{i=1}^n (x_{\mu}^{(\xi)} - 2\varepsilon_i)$  is an  $n$ -degree polynomial,

$$B(x)/A(x) = -\sum_{i=1}^n \frac{\Omega_i}{x_{\mu}^{(\xi)} - 2\varepsilon_i} - \frac{1}{G}, \quad (7)$$

$V(x)$  are called Van Vleck polynomials [40] of degree  $n-1$ , which are determined according to Eq. (6). They are defined as

$$V(x) = \sum_{i=0}^{n-1} b_i x^i. \quad (8)$$

The polynomials  $P(x)$  with zeros corresponding to the solutions of Eq. (4) is defined as

$$P(x) = \prod_{i=1}^k (x - x_i^{(\xi)}) = \sum_{i=0}^k a_i x^i, \quad (9)$$

where  $k$  is the number of pairs.  $b_i$  and  $a_i$  are the expansion coefficients to be determined instead of the Richardson variables  $x_i$ . Furthermore, if we set  $a_k = 1$  in  $P(x)$ , the coefficient  $a_{k-1}$  then equals the negative sum of the  $P(x)$  zeros,  $a_{k-1} = -\sum_{i=1}^k x_i^{(\xi)} = -E_k^{(\xi)}$ .

If the value of  $x$  approaches twice the single-particle energy of a given level  $\delta$ , i.e.,  $x = 2\varepsilon_{\delta}$ , one can rewrite Eq. (6) in doubly degenerate systems with  $\Omega_i = 1$  as [41, 43]

$$\left(\frac{P'(2\varepsilon_{\delta})}{P(2\varepsilon_{\delta})}\right)^2 - \frac{1}{G} \left(\frac{P'(2\varepsilon_{\delta})}{P(2\varepsilon_{\delta})}\right) = \sum_{i \neq \delta} \frac{\left[\left(\frac{P'(2\varepsilon_{\delta})}{P(2\varepsilon_{\delta})}\right) - \left(\frac{P'(2\varepsilon_i)}{P(2\varepsilon_i)}\right)\right]}{2\varepsilon_{\delta} - 2\varepsilon_i} \quad (10)$$

In Ref. [45], a new iterative algorithm is established for the exact solution of the standard pairing problem within the Richardson-Gaudin method using the polynomial approach in Eq. (10). It provides efficient and robust solutions for both spherical and deformed systems at a large scale. The key to its success is determining the initial guesses for the large-set nonlinear equations involved in a controllable and physically motivated manner. Moreover, one reduces the large-dimensional problem to a one-dimensional Monte Carlo sampling procedure, which improves the algorithm's efficiency and avoids the nonsolutions and numerical instabilities that persist in most existing approaches. Based on the new iterative algorithm, we applied the model to study the actinide nuclei isotopes, where an excellent agreement with experimental data was obtained [45–48].

## B. The Fourier shape parametrization

Recent studies demonstrated that the developed Fourier parametrization of deformed nuclear shapes was highly effective in capturing the essential features of nuclear shapes, particularly up to the scission configuration [22, 49]. Current research indicated that combining this innovative Fourier shape parametrization with the LSD + Yukawa-Folded macro-microscopic potential-energy framework was exceptionally efficient [47, 48, 50, 51]. This work primarily adopted the macro-microscopic framework outlined in Refs. [47, 48], where the single-particle energies  $\{\epsilon_i\}$  in the model Hamiltonian (1) were derived from the Yukawa-Folded potential.

The nuclear surface is expanded in terms of a Fourier series of dimensionless coordinates as follows:

$$\frac{\rho_s^2(z)}{R_0^2} = \sum_{n=1}^{\infty} \left[ a_{2n} \cos\left(\frac{(2n-1)\pi}{2} \frac{z - z_{\text{sh}}}{z_0}\right) + a_{2n+1} \sin\left(\frac{2n\pi}{2} \frac{z - z_{\text{sh}}}{z_0}\right) \right], \quad (11)$$

where  $\rho_s(z)$  is the distance from a surface point to the symmetry  $z$ -axis, and  $R_0 = 1.2A^{1/3}$  fm is the radius of a corresponding spherical shape with the same volume. The shape's extension along the symmetry axis is  $2z_0$ , with the left and right ends located at  $z_{\text{min}} = z_{\text{sh}} - z_0$  and  $z_{\text{max}} = z_{\text{sh}} + z_0$ , respectively. The parameter  $z_0$  represents half the shape's extension along the symmetry axis and is determined by volume conservation, while  $z_{\text{sh}}$  is set such that the center of mass of the nuclear shape is at the origin of the coordinate system. Based on the convergence properties discussed in Ref. [22], the first five terms  $a_2, \dots, a_6$  are retained as a starting point, and the parameters  $a_n$  are transformed into deformation parameters  $q_n$  as follows:

$$\begin{aligned} q_2 &= a_2^{(0)} / a_2 - a_2 / a_2^{(0)}, \\ q_3 &= a_3, \\ q_4 &= a_4 + \sqrt{(q_2/9)^2 + (a_4^{(0)})^2}, \\ q_5 &= a_5 - (q_2 - 2)a_3/10, \\ q_6 &= a_6 - \sqrt{(q_2/100)^2 + (a_6^{(0)})^2}, \end{aligned} \quad (12)$$

where  $a_n^{(0)}$  are the Fourier coefficients for the spherical shape. Higher-order coordinates  $q_5$  and  $q_6$  are generally set to zero within the accuracy of the current approach. The set of  $q_i$  parameters has explicit physical significance in describing the shape of the fissioning nucleus:  $q_2$  denotes the elongation,  $q_4$  represents the neck parameter, and  $q_3$  indicates the left-right asymmetry.

Additionally, the non-axial deformation of nuclear shapes is described as follows, assuming that the surface cross-section at a given  $z$ -coordinate is elliptical with semi-axes  $a(z)$  and  $b(z)$ :

$$\varrho_s^2(z, \varphi) = \rho_s^2(z) \frac{1 - \eta^2}{1 + \eta^2 + 2\eta \cos(2\varphi)}, \quad (13)$$

where  $\eta = \frac{b-a}{b+a}$  characterizes the non-axial deformation. Volume conservation requires that  $\rho_s^2(z) = a(z) + b(z)$ , with the condition  $ab = \rho_s^2(z)$  ensuring volume conservation for non-axial deformations. The semi-axes are then given by:

$$a(z) = \rho_s(z) \sqrt{\frac{1-\eta}{1+\eta}}, \quad b(z) = \rho_s(z) \sqrt{\frac{1+\eta}{1-\eta}}. \quad (14)$$

This description of non-axial shapes using the parameters  $q_2$  and  $\eta$  is more general than the commonly used Bohr parametrization  $(\beta, \gamma)$ . For spheroidal shapes, both descriptions are equivalent. However, as shown in Fig. 1, where the two parametrizations are compared, the periodicity of nuclear shapes by a  $60^\circ$  rotation angle is similar in both  $(q_2, \eta)$  and  $(\beta, \gamma)$  planes. It is important to note that this regularity is disrupted when higher multipolarity deformations  $q_n$  ( $n > 2$ ) are considered, making the  $(\eta, q_2, q_3, q_4, q_6)$  shape parametrization substantially more general than the 3-dimensional  $(\epsilon_2, \epsilon_4(\gamma), \gamma)$  parametrization used in Ref. [54, 55]. The two parametrizations coincide only in the special case of spheroidal shapes.

It is essential to stress that different points in the  $(\beta, \gamma)$ , and  $(q_2, \eta)$  planes can correspond to identical shapes when higher  $q_n$  ( $n > 2$ ) degrees of freedom are neglected, differing only in the interchange of coordinate system axes. For example, the point  $(\beta = 0.4, \gamma = 0)$  corresponds to  $(q_2 = 0.42, \eta = 0)$  in the new parametrization, representing the same shape as  $(\beta = 0.4, \gamma = 120^\circ)$ , which corresponds to  $(q_2 = -0.21, \eta = 0.16)$  in the new parametrization.

When analyzing potential energy landscapes that include triaxial degrees of freedom, it is crucial to avoid treating as distinct configurations points in the  $(q_2, \eta)$  deformation plane that are merely rotational images of each other at  $\gamma = 60^\circ$ .

In this study, the dynamic process of nuclear fission will be described in the three-dimensional deformation space  $(\eta, q_2, q_4)$  using the Fourier shape parametrization.

### C. The potential energy

This study calculated the PESs for the isotopes  $^{170}\text{Pt}$ ,  $^{172}\text{Hg}$ , and  $^{174}\text{Pb}$  in a three-dimensional deformation space  $(\eta, q_2, q_4)$  and analyzed the impact of pairing interactions on the shape coexistence of these isotopes. The results were obtained over the following grid points in the deformation parameter space:

$$\begin{aligned} \eta &\in [0.00, 0.20] & \Delta\eta &= 0.02 \\ q_2 &\in [-0.60, 0.85] & \Delta q_2 &= 0.05 \\ q_4 &\in [-0.30, 0.30] & \Delta q_4 &= 0.03. \end{aligned} \quad (15)$$

As indicated in the literature [22], the  $q_3$  degree of freedom has no significant impact on the description of shape coexistence for the isotopes discussed in this paper. Therefore, in this study,  $q_3$  was set to 0, and for each point on the PES,  $q_4$  was minimized to find the energy extremum. The potential energy of the system was calculated within the macro-microscopic approach in this work. The total energy  $E_{\text{total}}(N, Z, q_n)$  of a nucleus with a given deformation is calculated as

$$E_{\text{total}}(N, Z, q_n) = E_{\text{LD}}(N, Z, q_n) + E_{\text{B}}(N, Z, q_n), \quad (16)$$

where  $E_{\text{LD}}(N, Z, q_n)$  was the macroscopic term obtained by the LSD model with proton number  $Z$  and neutron number  $N$  [56]. In the current calculation for the potential-energy surface, we just considered the energy  $E_{\text{B}}(N, Z, q_n)$  related to the shape parameter  $\{q_2, q_4\}$ .

$$E_{\text{B}}(N, Z, q_n) = E_{\text{shell}}(N, Z, q_n) + E_{\text{pair}}(N, Z, q_n). \quad (17)$$

The microscopic term consisted of the shell correction energy  $E_{\text{shell}}^{\nu(\pi)}(N, Z, \{\epsilon_i\}, q_2, q_4)$  proposed by Strutinsky [57, 58], and the pairing interaction energy  $E_{\text{pair}}^{\nu(\pi)}(N, Z, \{\epsilon_i\}, q_2, q_4)$  calculated from Eq. (1). Here,  $\nu$  ( $\pi$ ) was the label of the neutron (proton) sector. In the current study, we considered 18 deformed harmonic-oscillator shells in Yukawa-Folded single-particle potential to obtain single-particle levels for the microscopic calculations. For the pairing interaction energy, we performed 29 single-particle levels around the neutron Fermi level and 22 single-particle levels around the proton Fermi level.

To validate our results and further explored the efficacy of the exactly solvable pairing model, we also calculated the PESs for the isotopes considered under the BCS approximation. The pairing interaction was determined as the difference between the BCS energy [24] and the single-particle energy sum and the average pairing energy [59].

$$E_{\text{pair}} = E_{\text{BCS}} - \sum_{i=1}^k \epsilon_i - \tilde{E}_{\text{pair}}. \quad (18)$$

In the BCS approximation the ground-state energy of a system with an even number of particles and a monopole pairing

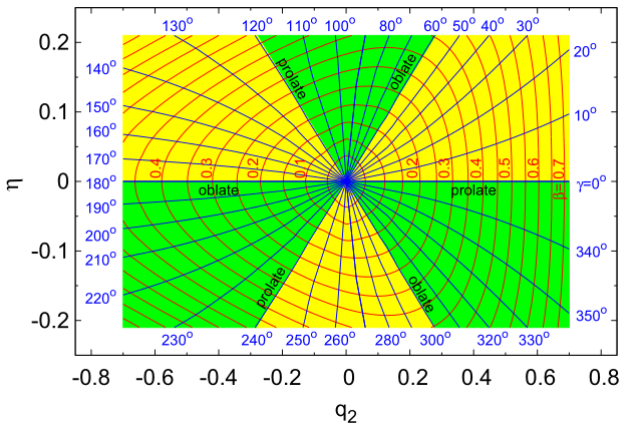


Fig. 1. Relationsheep between the elongation parameter  $q_2$  and the nonaxiality parameter  $\eta$  [22, 49], and the traditional Bohr deformation parameters  $\beta$  and  $\gamma$  is taken from [52, 53].



force was given by

$$E_{\text{BCS}} = \sum_{i=1}^k 2\varepsilon_i v_i^2 - G \left( \sum_{i=1}^k u_i v_i \right)^2 - G \sum_{i=1}^k v_i^4, \quad (19)$$

where the sums run over the pairs of single-particle states contained in the pairing window defined below. The coefficients  $v_i$  and  $u_i = \sqrt{1 - v_i^2}$  were the BCS occupation amplitudes.

The average projected pairing energy, for a pairing window of width  $2\Omega$ , which is symmetric in energy with respect to the Fermi energy, is equal to

$$\begin{aligned} \tilde{E}_{\text{pair}} = & -\frac{1}{2}\tilde{g}\tilde{\Delta}^2 + \frac{1}{2}\tilde{g}G\tilde{\Delta} \arctan\left(\frac{\Omega}{\tilde{\Delta}}\right) - \log\left(\frac{\Omega}{\tilde{\Delta}}\right)\tilde{\Delta} \\ & + \frac{3}{4}G \frac{\Omega/\tilde{\Delta}}{1 + (\Omega/\tilde{\Delta})^2} / \arctan\left(\frac{\Omega}{\tilde{\Delta}}\right) - \frac{1}{4}G, \end{aligned} \quad (20)$$

Here  $\tilde{g}$  was the average single-particle level density and  $\tilde{\Delta}$  the average pairing gap corresponding to a pairing strength  $G$

$$\tilde{\Delta} = 2\Omega \exp\left(-\frac{1}{G\tilde{g}}\right). \quad (21)$$

#### D. Influence of pairing interactions on the shape coexistence of $^{170}\text{Pt}$ , $^{172}\text{Hg}$ and $^{174}\text{Pb}$ isotopes

Figure 2 shows the PESs of  $^{170}\text{Pt}$  projected onto the  $(q_2, \eta)$  plane for different pairing interaction strengths  $G^\nu$  (MeV), while the proton pairing interaction strength is fixed at  $G^\pi = 0.100$  MeV.  $G^\nu$  and  $G^\pi$  represent the neutron and proton pairing interaction strengths (MeV), respectively. The energy is minimized in the  $q_4$  direction and  $q_3$  is set to 0 and normalized to zero energy at the ground-state value. The choice of  $G^\nu$  varying from 0.03 to 0.145 MeV, and  $G^\pi = 0.100$  MeV, were based on the fact that our calculations in the next section, when employing  $G^\nu = 0.145$  MeV, and  $G^\pi = 0.100$  MeV, closely matched the experimental odd-even mass differences for the  $^{171}\text{Pt}$  to  $^{180}\text{Pt}$  isotopes. Therefore, this range was selected to study the effects of pairing strength variations on the shape coexistence. The red lines represent the corresponding  $(\beta, \gamma)$  coordinates, with  $\gamma$  coordinates distributed within  $0 \leq \gamma \leq 180^\circ$ . The  $\beta$  coordinate values are taken as 0.1, 0.2, 0.3..., etc.

In Figures 2 (a)-(d), the PESs of  $^{170}\text{Pt}$  are shown for different values of the neutron pairing interaction strength  $G^\nu$ , while the proton pairing interaction strength is fixed at  $G^\pi = 0.100$  MeV. The values of  $G^\nu$  are: 0.030, 0.070, 0.105, and 0.145 MeV. It can be seen that the ground-state of the  $^{170}\text{Pt}$  isotope is located at  $(q_2 \approx 0.150, \eta = 0)$ , indicating a prolate shape for different pairing strengths. The other minimum at  $(q_2 \approx -0.150, \eta = 0.04, \gamma = 120^\circ)$  illustrated in Figure 2 is simply a reflection of the ground-state minimum.

It is noteworthy to highlight the existence of two distinct shape isomers in  $^{170}\text{Pt}$  with different pairing strengths. The first is an oblate shape isomer located at  $(q_2 = -0.400, \eta = 0)$ , with an energy approximately 3.900 MeV above the ground-state. The second is a triaxial shape isomer at  $(q_2 \approx 0.600, \eta \approx 0.060 (\gamma \approx 10^\circ))$ , positioned around 4.0 MeV above the ground-state. These isomers represent the local minima on the potential energy surface that are separated from the ground-state by energy barriers, highlighting the complex deformation characteristics of the nucleus. With an increase in pairing strength, both shape isomers become shallower. When the pairing strength  $G^\nu$  reaches 0.145 MeV, the oblate isomer disappears (see Fig. 2 (d)).

As shown in Figures 3 (a)-(d), the PESs for different pairing interaction strengths demonstrates the evolution of the triaxial minimum at  $(q_2 = 0.150, \eta = 0.020)$  to the oblate minimum at  $(q_2 = 0.100, \eta = 0.040)$  as the pairing interaction strength increases. The nucleus of  $^{172}\text{Hg}$  is nearly  $\gamma$ -unstable, with the energy difference between different points in the ground-state valley not exceeding approximately 0.4 MeV. Additionally, three shape isomers are visible in the (a)-(d) maps: a prolate isomer at  $(q_2 \approx 0.600, \eta = 0)$ ,  $E \approx 5.0$  MeV; a triaxial isomer at  $(q_2 \approx 0.400, \eta = 0.100)$ ,  $E \approx 4.0$  MeV, and oblate one at  $(q_2 \approx -0.45, \eta = 0)$ ,  $E \approx 4.0$  MeV. These local minima are separated by energy barriers of approximately 1 MeV in height. As the pairing strength increases, all shape isomers gradually become shallower. By  $G^\nu = 0.145$  MeV and  $G^\pi = 0.100$  MeV (Figure 3 (d)), the triaxial isomer at  $(q_2 \approx 0.400, \eta = 0.100)$  disappeared.

The PESs of  $^{174}\text{Pb}$ , as presented in Figures 4 (a)-(d), reveal that a prolate ground-state  $(q_2 \approx 0.150, \eta = 0)$  (in Fig. 4 (a)) tend to become spherical (in Fig. 4 (d)) as the pairing interaction strength increases. The shape isomers observed here are particularly interesting: a prolate shape at  $(q_2 = 0.600, \eta = 0, E \approx 5.0$  MeV and a slightly triaxial oblate shape at  $(q_2 = 0.450, \eta = 0.020, E \approx 3.9$  MeV in Fig. 4 (a), and (b), respectively. As the pairing strength increased, both shape isomers gradually became shallower. When  $G^\nu = 0.145$  MeV, and  $G^\pi = 0.100$  MeV (Figure 4 (d)), they almost disappeared. Overall, regardless of pairing strength, there was no indication of robust shape coexistence in this nucleus.

Figures 5 illustrate the PESs projections of  $^{170}\text{Pt}$ ,  $^{172}\text{Hg}$ , and  $^{174}\text{Pb}$  under realistic pairing interaction strengths, with  $G^\nu = 0.145$  MeV, and  $G^\pi = 0.100$  MeV under both Exact and BCS pairing schemes.

As shown in Figure 5, the ground-state of  $^{170}\text{Pt}$  is prolate, located at  $(q_2 = 0.15, \eta = 0)$  under both the Exact and BCS pairing schemes. However, BCS pairing exhibited a shallower depth for the prolate minimum compared with Exact pairing, indicating a less pronounced prolate ground-state. Furthermore, a triaxial isomer appeared at  $(q_2 \approx 0.600, \eta \approx 0.060 (\gamma \approx 10^\circ))$  under Exact pairing, whereas it was less distinguishable in the BCS case.

The ground-state of  $^{172}\text{Hg}$  (Fig. 5) is found at  $(q_2 = 0.10, \eta \approx 0.04)$  as an oblate minimum, with another minimum at  $(q_2 \approx -0.100, \eta \approx 0.02)$ , which exhibits  $\gamma$ -unstable

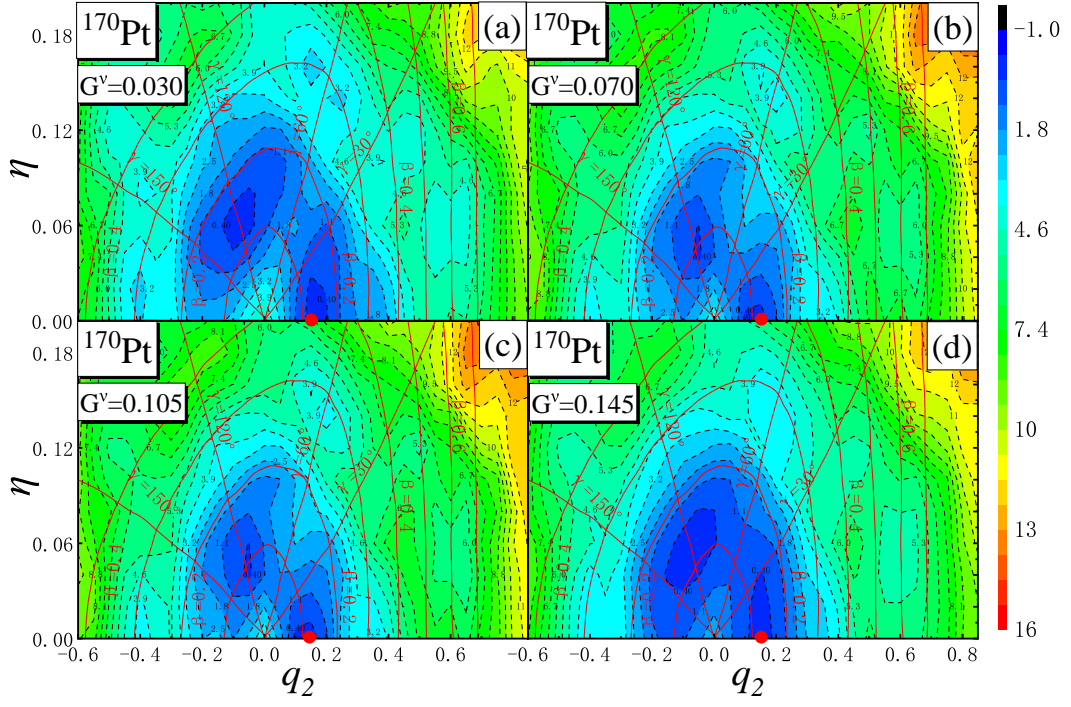


Fig. 2. Potential energy surface of  $^{170}\text{Pt}$  projected onto the  $(q_2, \eta)$  plane under different pairing interaction strengths  $G^\nu$  (MeV), while the proton pairing interaction strength is fixed at  $G^\pi = 0.100$  MeV. The energy is minimized in the  $q_4$  direction and  $q_3$  is set to 0 and normalized to zero energy at the ground-state value. The ground-state deformation is represented by a red dot.

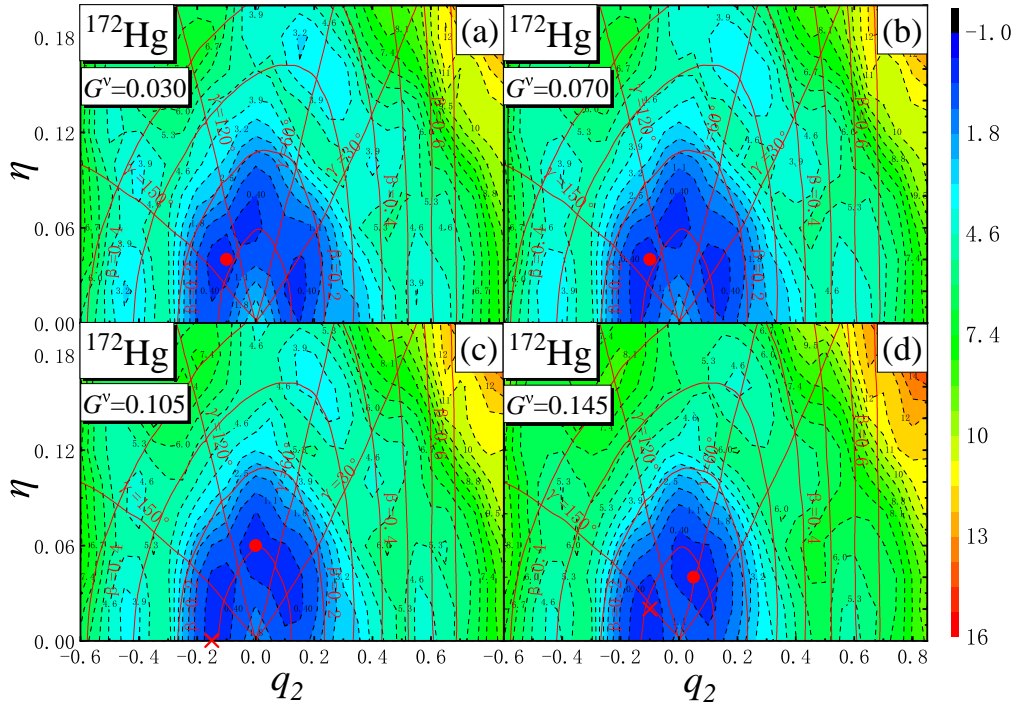


Fig. 3. Same as Fig. 2, but for  $^{172}\text{Hg}$ .

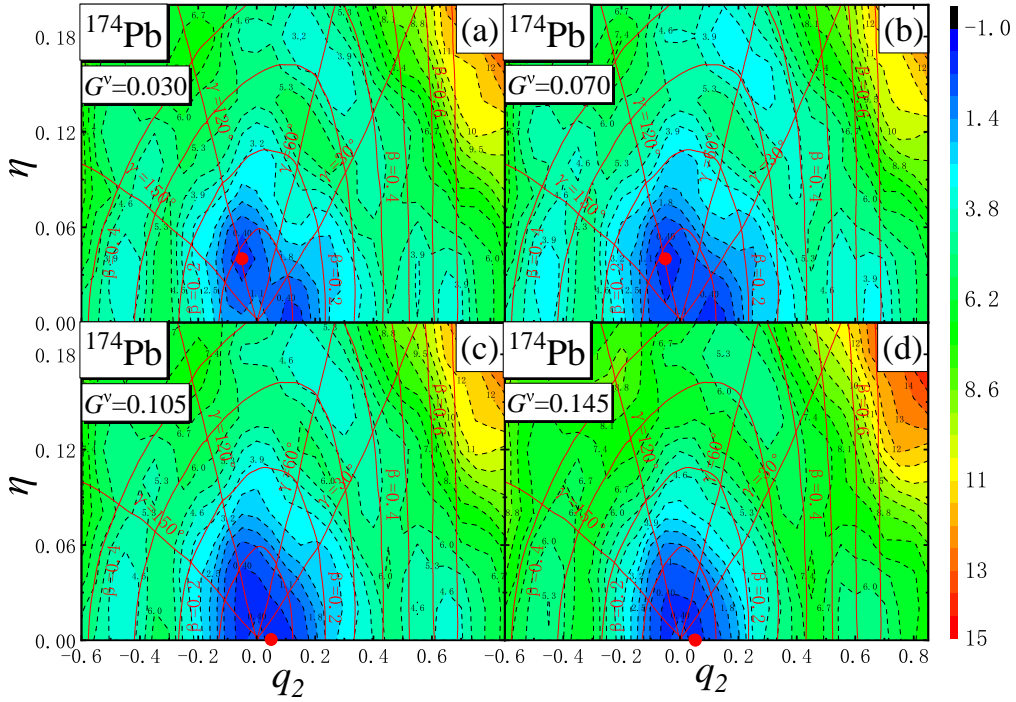


Fig. 4. Same as Figs. 2 and 3, but for  $^{174}\text{Pb}$ .

deformation. The PES of  $^{172}\text{Hg}$  provides an excellent example of an almost  $\gamma$ -unstable nucleus. Under Exact pairing, this  $\gamma$ -unstable minimum is more symmetric, with clear reflections around  $\gamma = 150^\circ$ ,  $\gamma = 30^\circ$ , and  $\gamma = 90^\circ$ . Under BCS pairing, the  $\gamma$ -unstable features are less prominent, and the oblate minimum becomes more dominant. Additionally, two shape isomers are visible under Exact pairing model: a prolate isomer at  $(q_2 \approx 0.600, \eta = 0)$ ,  $E \approx 4.6$  MeV, and an oblate one at  $(q_2 \approx -0.45, \eta = 0)$ ,  $E \approx 4.6$  MeV. However, these changes were not distinguishable in the BCS case.

As shown in Figures 5 (c), the ground-state shape of  $^{174}\text{Pb}$  tended to be spherical. The PES under Exact pairing revealed a nearly spherical configuration with minor prolate and oblate shape isomers. In contrast, BCS pairing resulted in a more pronounced spherical minimum and diminishes the depth of shape isomers.

In summary, as the number of protons increases, the ground-state transitions from prolate for  $^{170}\text{Pt}$  to the coexistence of  $\gamma$ -unstable and oblate for  $^{172}\text{Hg}$ , eventually approached a nearly spherical configuration for  $^{174}\text{Pb}$ . The comparison between Exact and BCS pairing demonstrates that BCS pairing tends to smooth out shape coexistence and reduce the depth of shape isomer, leading to less pronounced deformation features. The differences in results between Exact and BCS pairing may be attributed to the mean-field approximation in the BCS approach, which likely simplifies the treatment of pairing interactions. This approximation is thought to smooth out shape coexistence phenomena by suppressing pairing fluctuations, energy gaps, and shell effects, potentially leading to less pronounced deformation features.

#### E. Shape coexistence analysis in the Pt isotope chain

In this paper, we investigate the PESs of the even-even  $^{170-180}\text{Pt}$  isotopes using the exactly solvable deformed mean-field plus pairing model. Our analysis provides a comprehensive examination of the shape coexistence phenomena across these isotopes.

The pairing interaction strength, denoted as  $G$ , serves as the sole adjustable parameter within our model. It is typically determined either through empirical formulas or by fitting to experimental odd-even mass differences [60, 61]. In this study, we determined  $G^\nu$  by fitting the experimental odd-even mass differences for the  $^{171-180}\text{Pt}$  isotope chain and  $G^\pi$  by fitting the experimental odd-even mass differences for the  $^{174}\text{Pt}$  to  $^{178}\text{Pb}$  isotonic chain. The odd-even mass differences are computed using the following expression:

$$P(A) = E_{\text{total}}(N+1, Z) + E_{\text{total}}(N-1, Z) - 2E_{\text{total}}(N, Z).$$

This quantity is highly sensitive to variations in the pairing interaction strength  $G$  [62], due to the pairing interaction between nucleons. As shown in Fig. 6, by employing  $G^\nu = 0.145$  MeV and  $G^\pi = 0.100$  MeV, our calculations closely reproduced the experimental odd-even mass differences for the  $^{171-180}\text{Pt}$  isotopes, yielding a root mean square deviation of  $\sigma = 0.465$  MeV. Additionally, as display in Fig. 7 for the  $^{174}\text{Pt}$  to  $^{178}\text{Pb}$  isotonic chain, the calculations closely matched the experimental odd-even mass differences,

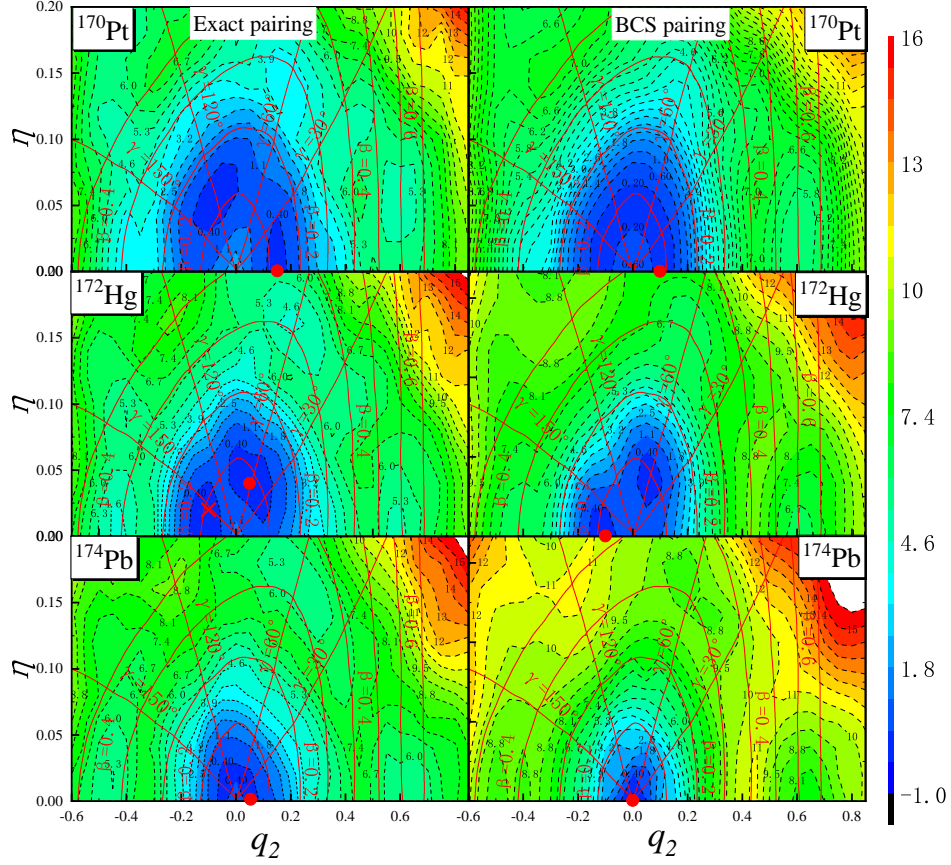
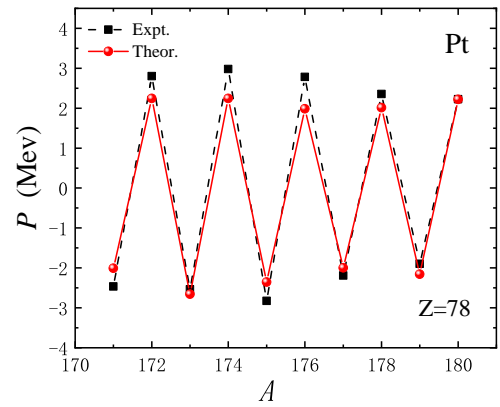


Fig. 5. Potential energy surfaces of  $^{170}\text{Pt}$ ,  $^{172}\text{Hg}$  and  $^{174}\text{Pb}$  projected on the  $(q_2, \eta)$  plane under both Exact and BCS pairing schemes, with the energy minimized in the  $q_4$  direction,  $q_3$  set to 0 and normalized to zero energy at the ground-state value. The realistic pairing interaction strengths  $G^\nu = 0.145$  MeV, and  $G^\pi = 0.100$  MeV are adopted. The ground-state deformation is represented by a red dot, while the coexistence minimum is indicated by a red cross.

with a root mean square deviation of  $\sigma = 1.192$  MeV.

$$\sigma = \sqrt{\sum_{\mu=1}^{\mathcal{N}} (P_{\mu}^{\text{Theor.}} - P_{\mu}^{\text{Expt.}})^2 / \mathcal{N}}. \quad (22)$$

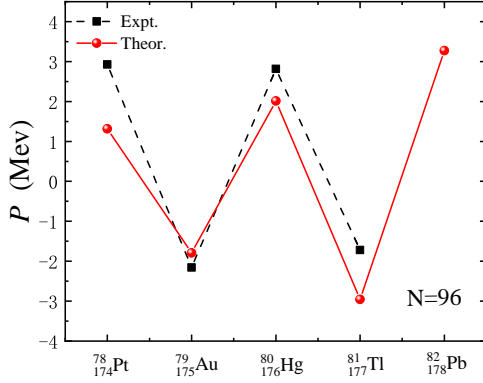


481

Fig. 6. Odd-even mass differences (in MeV) for Pt isotopes. "Expt." represents experimental values, and "Theor." represents theoretical values. Experimental data are from [62].

Here,  $P_{\mu}^{\text{Theor.}}$  and  $P_{\mu}^{\text{Expt.}}$  represent the theoretical and experimental values of the odd-even mass differences, respectively, and  $\mathcal{N}$  denotes the total number of data points.





485

486 Fig. 7. Odd-even mass differences (in MeV) for the  $^{174}\text{Pt}$  to  $^{178}\text{Pb}$   
 487 isotonic chain. "Expt." represents experimental values, and "Theor."  
 488 represents theoretical values. Experimental data are from [62].

489 Next, we examine the PES of the  $^{170-180}\text{Pt}$  even-even  
 490 isotopes under the determined pairing interaction strengths  
 491  $G^\nu = 0.145$  MeV and  $G^\pi = 0.100$  MeV. Figure 8 shows the  
 492 PES projected onto the  $(q_2, \eta)$  plane. For  $^{170}\text{Pt}$ , the ground-  
 493 state exhibited a prolate deformation at  $(q_2 = 0.15, \eta = 0)$ .  
 494 In contrast, for  $^{172}\text{Pt}$ , a more deformed minimum emerged,  
 495 leading to the coexistence of a triaxial shape ( $\gamma \approx 30^\circ$ )  
 496 and a nearly prolate-deformed minimum at  $(\gamma \approx 120^\circ)$ , in-  
 497 dicative of  $\gamma$ -instability due to the presence of multiple low-  
 498 energy configurations at different  $\gamma$  values. The triaxial shape  
 499 is even more pronounced in  $^{174}\text{Pt}$ , where the ground-state  
 500 is triaxial with deformation parameters  $(q_2 = 0.020, \eta =$   
 501  $0.10, \beta \approx 0.2, \gamma \approx 90^\circ)$  and a coexisting prolate minimum  
 502 at  $(q_2 = 0.15, \eta = 0)$ . In  $^{176}\text{Pt}$  a  $\gamma$ -unstable ground-state and  
 503 a prolate minimum coexisted, but by  $^{178}\text{Pt}$  and  $^{180}\text{Pt}$ , a well-  
 504 deformed prolate minimum quickly developed, becoming the  
 505 most pronounced prolate ground-state at the mid-shell.

506 The findings of this study are broadly consistent with the  
 507 results of Ref. [20], which studied the  $^{172-194}\text{Pt}$  isotopic  
 508 chain in the framework of the interacting boson model and  
 509 self-consistent HFB calculation using the Gogny-D1S in-  
 510 teraction. Both studies identified shape coexistence in the  
 511  $^{172-176}\text{Pt}$  region, with  $\gamma$ -unstable minima and triaxial shapes  
 512 in  $^{174}\text{Pt}$ . Additionally, both studies showed the dominance  
 513 of prolate deformation in  $^{178}\text{Pt}$ , and  $^{180}\text{Pt}$ , with the prolate  
 514 minimum becoming the most pronounced ground state at the  
 515 mid-shell.

516 It is noteworthy that a triaxial shape isomer exists for  
 517  $^{170-174}\text{Pt}$ , characterized by  $(q_2 \approx 0.600, \eta \approx 0.060$  ( $\gamma \approx$   
 518  $10^\circ)$ ), and positioned approximately 5.0 MeV above the  
 519 ground-state. However, this triaxial shape isomer vanishes  
 520 for  $^{176-180}\text{Pt}$ .

521

### III. CONCLUSION

522 In this study, we systematically investigated the shape co-  
 523 existence phenomenon in isotopes near the magic proton  
 524 number of  $Z = 82$ , focusing specifically on the nuclei  $^{170}\text{Pt}$ ,  
 525  $^{172}\text{Hg}$ , and  $^{174}\text{Pb}$ , as well as the Pt isotopic chain from  $^{170}\text{Pt}$   
 526 to  $^{180}\text{Pt}$ . Our analysis, using a macro-microscopic approach  
 527 that combines the LSD model with a Yukawa-Folded poten-  
 528 tial and pairing corrections, revealed significant insights into  
 529 the impact of pairing interactions on nuclear shape evolution.

530 The PES of  $^{170}\text{Pt}$  revealed a prolate ground-state with ad-  
 531 ditional triaxial and oblate shape isomers. Both shape iso-  
 532 mers become progressively shallower with increasing neu-  
 533 tron pairing strength  $G^\nu$ , and the oblate isomer vanishes at  
 534  $G^\nu = 0.145$  MeV, indicating a significant dependence of  
 535 shape isomers on pairing strength. The ground-state deforma-  
 536 tion of  $^{172}\text{Hg}$  transitions from triaxial to oblate with increas-  
 537 ing  $G^\nu$ , reflecting its nearly  $\gamma$ -unstable nature. Three shape  
 538 isomers (prolate, triaxial, and oblate) were observed, with  
 539 energy barriers separating these configurations. As  $G^\nu$  in-  
 540 creased, the triaxial isomer disappeared at  $G^\nu = 0.145$  MeV,  
 541 demonstrating the impact of pairing interactions on shape sta-  
 542 bility.  $^{174}\text{Pb}$  exhibited a prolate ground-state that became in-  
 543 creasingly spherical with stronger pairing interactions. While  
 544 shape isomers are present at weaker pairing strengths, their  
 545 prominence diminishes significantly, and robust shape coex-  
 546 istence was not observed in this nucleus.

547 For realistic pairing interaction, the ground-state shapes  
 548 transition from prolate in  $^{170}\text{Pt}$  to a coexistence of  $\gamma$ -unstable  
 549 and oblate shapes in  $^{172}\text{Hg}$ , ultimately approaching spheri-  
 550 cal symmetry in  $^{174}\text{Pb}$ . This progression highlights the in-  
 551 terplay between proton number and pairing interactions in  
 552 shaping nuclear deformation. The comparison between Exact  
 553 and BCS pairing for realistic  $^{170}\text{Pt}$ ,  $^{172}\text{Hg}$ , and  $^{174}\text{Pb}$  demon-  
 554 strated that BCS pairing tends to smooth out shape coexis-  
 555 tence and reduce the depth of shape isomers, leading to less  
 556 pronounced deformation features.

557 These findings emphasize the critical role of pairing inter-  
 558 actions in shaping nuclear deformation landscapes and shape  
 559 coexistence, offering deeper insights into the structural evo-  
 560 lution of nuclei near the mid-shell region. This study con-  
 561 tributes valuable theoretical perspectives to the understand-  
 562 ing of nuclear shape phenomena and the influence of pairing  
 563 interactions on nuclear dynamics.

564 Based on the analysis of the PESs for the even-even  
 565  $^{170-180}\text{Pt}$  isotopes, the results show significant shape evo-  
 566 lution across the isotopic chain. For  $^{170}\text{Pt}$ , the ground-state  
 567 exhibited prolate deformation, with deformation parameters.  
 568 However, for  $^{172}\text{Pt}$ , a more deformed minimum appears, lead-  
 569 ing to the coexistence of a triaxial shape and a nearly prolate-  
 570 deformed minimum. The triaxial shape becomes even more  
 571 pronounced in  $^{174}\text{Pt}$ , where the ground-state is triaxial with  
 572 deformation parameters, coexisting with a prolate minimum.  
 573 For  $^{176}\text{Pt}$ , a  $\gamma$ -unstable ground-state coexists with a prolate  
 574 minimum. By  $^{178}\text{Pt}$ , and  $^{180}\text{Pt}$ , a well-deformed prolate mi-  
 575 nimum develops rapidly, becoming the most pronounced pro-  
 576 late ground-state in the mid-shell.

577 These results highlight the complex shape evolution in the  
 578 Pt isotopes, with shape coexistence and  $\gamma$ -instability playing  
 579 significant roles in the nuclear structure evolution, particu-  
 580 larly around the mid-shell region where prolate deformation  
 581 dominates.

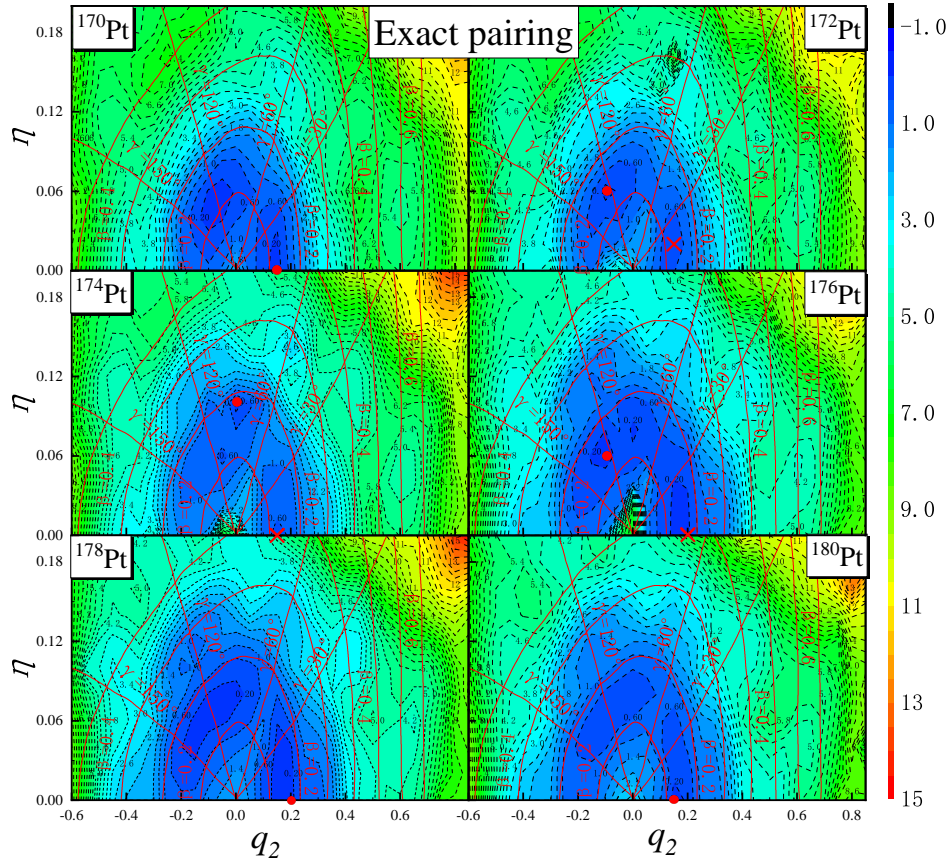


Fig. 8. Potential energy surfaces of the  $^{170-180}\text{Pt}$  even-even isotopes chain, projected on the  $(q_2, \eta)$  plane using the exact pairing model, where the energy is minimized in the  $q_4$  direction with  $q_3$  set to 0, with neutron and proton pairing interaction strengths of  $G^\nu = 0.145$  MeV,  $G^\pi = 0.100$  MeV. The ground-state deformation is represented by a red dot, while the coexistence minimum is indicated by a red cross.

- [1] K. Heyde, and J. L. Wood, Publisher's Note: Shape coexistence in atomic nuclei. *Rev. Mod. Phys.* **83**, 1467 (2011). doi: <http://dx.doi.org/10.1103/RevModPhys.83.1655>
- [2] J. Y. Jia, G. Giacalone, B. Bally, et al., Imaging the initial condition of heavy-ion collisions and nuclear structure across the nuclide chart. *Nucl. Sci. Tech.* **35**, 220 (2024). doi: <https://doi.org/10.1007/s41365-024-01589-w>
- [3] M. Q. Ding, D. Q. Fang, and Y. G. Ma, Neutron skin and its effects in heavy-ion collisions. *Nucl. Sci. Tech.* **35**, 211 (2024). doi: <https://doi.org/10.1007/s41365-024-01584-1>
- [4] B. S. Cai, and C. X. Yuan, Random forest-based prediction of decay modes and half-lives of superheavy nuclei. *Nucl. Sci. Tech.* **34**, 204 (2023). doi: <https://doi.org/10.1007/s41365-023-01354-5>
- [5] J. L. Huang, H. Wang, Y. G. Huang, et al., Prediction of  $(n, 2n)$  reaction cross-sections of long-lived fission products based on tensor model. *Nucl. Sci. Tech.* **35**, 184 (2024). doi: <https://doi.org/10.1007/s41365-024-01556-5>
- [6] Y. Liu, F. R. Xu, and Z. B. Cao, Shape Coexistence in Selenium Isotopes. *Nucl. Phys. Rev.* **27**, 2 (2010). DOI: 10.11804/NuclPhysRev.27.02.146
- [7] J. Rainwater, Nuclear Energy Level Argument for a Spheroidal Nuclear Model. *Phys. Rev.* **79**, 432 (1950). doi: <https://doi.org/10.1103/PhysRev.79.432>
- [8] A. Bohr, and B. R. Mottelson, Collective and individual-particle aspects of nuclear structure, *Dan. Mat. Fys. Medd.* **27**, 16 (1953).
- [9] A. Bohr, and B. R. Mottelson, Moments of Inertia of Rotating Nuclei. *Dan. Mat. Fys. Medd.* **30**, 1 (1955).
- [10] A. Arima, and H. Horie, Configuration Mixing and Magnetic Moments of Odd Nuclei. *Prog. Theor. Phys.* **12**, 623 (1954). doi: <https://doi.org/10.1143/PTP.12.623>
- [11] S. G. Nilsson, Binding states of individual nucleons in strongly deformed nuclei. *Dan. Mat. Fys. Medd.* **29**, 16 (1955).
- [12] H. Morinaga, Interpretation of Some of the Excited States of  $4n$  Self-Conjugate. *Phys. Rev.* **101**, 254 (1956). doi: <https://doi.org/10.1103/PhysRev.101.254>
- [13] J. P. Elliott, Collective motion in the nuclear shell model. I. Classification schemes for states of mixed

- configurations. *Proc. R. Soc. A* **245**, 128. doi: <https://doi.org/10.1098/rspa.1958.0072>
- [14] P. Möller, A. J. Sierk, R. Bengtsson et al., Global Calculation of Nuclear Shape Isomers. *Phys. Rev. Lett.* **103** 212501 (2009). doi: [10.1103/PhysRevLett.103.212501](https://doi.org/10.1103/PhysRevLett.103.212501)
- [15] M. Siciliano, I. Zanon, A. Goasduff et al., Shape coexistence in the neutron-deficient  $^{188}\text{Hg}$  investigated via lifetime measurements. *Phys. Rev. C* **102**, 014318 (2020). doi: <https://doi.org/10.1103/PhysRevC.102.014318>
- [16] R. Julin, T. Grahn, J. Pakarinen et al., In-beam spectroscopic studies of shape coexistence and collectivity in the neutron-deficient  $Z \approx 82$  nuclei. *J. Phys. G* **43**, 024004 (2016). doi: [10.1088/0954-3899/43/2/024004](https://doi.org/10.1088/0954-3899/43/2/024004)
- [17] M. Bender, P. H. Heenen, and P. G. Reinhard, Self-consistent mean-field models for nuclear structure. *Rev. Mod. Phys.* **75**, 121 (2003). doi: <https://doi.org/10.1103/RevModPhys.75.121>
- [18] T. Nikšić, D. Vretenar, P. Ring et al., Shape coexistence in the relativistic Hartree-Bogoliubov approach. *Phys. Rev. C* **65**, 054320 (2002). doi: <https://doi.org/10.1103/PhysRevC.65.054320>
- [19] F. Z. Xing, J. P. Cui, Y. H. Gao et al., Structure and  $\alpha$  Decay of Superheavy Nucleus  $^{296}\text{Og}$ . *Nucl. Phys. Rev.* **40**, 4 (2023). doi: [10.11804/NuclPhysRev.40.2023059](https://doi.org/10.11804/NuclPhysRev.40.2023059)
- [20] J. E. García-Ramos, K. Heyde, L. M. Robledo et al., Shape evolution and shape coexistence in Pt isotopes: Comparing interacting boson model configuration mixing and Gogny mean-field energy surfaces. *Phys. Rev. C* **98**, 034313 (2014). doi: [10.1103/PhysRevC.98.034313](https://doi.org/10.1103/PhysRevC.98.034313)
- [21] J. E. García-Ramos, and K. Heyde, Nuclear shape coexistence: A study of the even-even Hg isotopes using the interacting boson model with configuration mixing. *Phys. Rev. C* **89**, 014306 (2014). doi: [10.1103/PhysRevC.89.014306](https://doi.org/10.1103/PhysRevC.89.014306)
- [22] K. Pomorski, B. Nerlo-Pomorska, A. Dobrowolski, et al. Shape isomers in Pt, Hg and Pb isotopes with  $N \leq 126$ . *Eur. Phys. J. A*, **56**, 107 (2020). doi: [10.1140/epja/s10050-020-00115-x](https://doi.org/10.1140/epja/s10050-020-00115-x)
- [23] T. Kibedi, and C. M. Baglin, ENSDEF (2010), <http://www.nndc.bnl.gov/ensdf>
- [24] J. Bardeen, L. N. Cooper, and J. R. Schrieffer, Theory of Superconductivity. *Phys. Rev.* **108**, 1175 (1957). doi: <https://doi.org/10.1103/PhysRev.108.1175>
- [25] A. Bohr, B. R. Mottelson, and D. Pines, Possible Analogy between the Excitation Spectra of Nuclei and Those of the Superconducting Metallic State. *Phys. Rev.* **110**, 4 (1958). doi: <https://doi.org/10.1103/PhysRev.110.936>
- [26] S. T. Belyaev, Effect of pairing correlations on nuclear properties. *Dan. Mat. Fys. Medd.* **31**, 11 (1959). doi: <https://www.osti.gov/biblio/4262925>
- [27] Y. Z. Wang, F. Z. Xing, J. P. Cui et al., Roles of tensor force and pairing correlation in two-proton radioactivity of halo nuclei. *Chin. Phys. C* **47**, 084101 (2023). doi: [10.1088/1674-1137/acd680](https://doi.org/10.1088/1674-1137/acd680)
- [28] Y. Z. Wang, F. Z. Xing, W. H. Zhang et al., Tensor force effect on two-proton radioactivity of  $^{18}\text{Mg}$  and  $^{20}\text{Si}$ . *Phys. Rev. C* **110**, 064305 (2024). doi: <https://doi.org/10.1103/PhysRevC.110.064305>
- [29] Y. Z. Wang, L. Yang, C. Qi et al., Pairing Effects on Bubble Nuclei. *Chin. Phys. Lett.* **36**, 032101 (2019). doi: [10.1088/0256-307X/36/3/032101](https://doi.org/10.1088/0256-307X/36/3/032101)
- [30] Y. Z. Wang, Z. Y. Hou, Q. L. Zhang et al., Effect of a tensor force on the proton bubble structure of  $^{206}\text{Hg}$ . *Phys. Rev. C* **91**, 017302 (2015). doi: <https://doi.org/10.1103/PhysRevC.91.017302>
- [31] J. Rissanen, R. M. Clark, A. O. Macchiavelli et al., Effect of the reduced pairing interaction on  $\alpha$ -decay half-lives of multi-quasiparticle isomeric states. *Phys. Rev. C* **90**, 044324 (2014). doi: <https://doi.org/10.1103/PhysRevC.90.044324>
- [32] N. Sandulescu, and G. F. Bertsch, Accuracy of BCS-based approximations for pairing in small Fermi systems nuclei. *Phys. Rev. C* **78**, 064318 (2008). doi: <https://doi.org/10.1103/PhysRevC.78.064318>
- [33] I. Talmi, Simple Models of Complex Nuclei. (Harwood Academic Publishers, Switzerland) (1993). doi: <https://doi.org/10.1201/9780203739716>
- [34] T. Otsuka, Y. Tsunoda, T. Abe, et al., Underlying Structure of Collective Bands and Self-Organization in Quantum Systems. *Phys. Rev. Lett.* **123**, 222502 (2019). doi: <https://doi.org/10.1103/PhysRevLett.123.222502>
- [35] Y. X. Yu, Y. Lu, G. J. Fu, et al., Nucleon-pair truncation of the shell model for medium-heavy nuclei. *Phys. Rev. C* **106**, 044309 (2022). doi: <https://doi.org/10.1103/PhysRevC.106.044309>
- [36] R. W. Richardson, A restricted class of exact eigenstates of the pairing-force Hamiltonian. *Phys. Lett.* **3**, 3277 (1963). doi: [https://doi.org/10.1016/0031-9163\(63\)90259-2](https://doi.org/10.1016/0031-9163(63)90259-2); Application to the exact theory of the pairing model to some even isotopes of lead. *Phys. Lett.* **5**, 82 (1963). doi: [https://doi.org/10.1016/S0375-9601\(63\)80039-0](https://doi.org/10.1016/S0375-9601(63)80039-0); R. W. Richardson and N. Sherman, Exact eigenstates of the pairing-force Hamiltonian. *Nucl. Phys.* **52**, 221 (1964). doi: [https://doi.org/10.1016/0029-5582\(64\)90687-X](https://doi.org/10.1016/0029-5582(64)90687-X); Pairing models of  $\text{Pb}^{206}$ ,  $\text{Pb}^{204}$  and  $\text{Pb}^{202}$ . *Nucl. Phys.* **52**, 253 (1964). doi: [https://doi.org/10.1016/0029-5582\(64\)90690-X](https://doi.org/10.1016/0029-5582(64)90690-X)
- [37] M. Gaudin, Diagonalization of a class of spin Hamiltonians. *Phys. J.* **37**, 1087 (1976). doi: <https://www.osti.gov/etdweb/biblio/7120011>
- [38] F. Pan, J. P. Draayer, and W. E. Ormand, A particle-number-conserving solution to the generalized pairing problem. *Phys. Lett. B* **422**, 1 (1998). doi: [https://doi.org/10.1016/S0370-2693\(98\)00034-3](https://doi.org/10.1016/S0370-2693(98)00034-3)
- [39] J. Dukelsky, C. Echebbag, and S. Pittel, Electrostatic mapping of nuclear pairing. *Phys. Rev. Lett.* **88**, 062501 (2002). doi: <https://doi.org/10.1103/PhysRevLett.88.062501>; J. Dukelsky, S. Pittel, G. Sierra, Colloquium: Exactly solvable Richardson-Gaudin models for many-body quantum systems. *Rev. Mod. Phys.* **76**, 643 (2004). doi: <https://doi.org/10.1103/RevModPhys.76.643>
- [40] X. Guan, K. D. Launey, M. X. Xie et al., Heine-Stieltjes correspondence and the polynomial approach to the standard pairing problem. *Phys. Rev. C* **86**, 024313 (2012). doi: <https://doi.org/10.1103/PhysRevC.86.024313>
- [41] A. Faribault, O. E. Araby, C. Sträter et al., Gaudin models solver based on the correspondence between Bethe ansatz and ordinary differential equations. *Phys. Rev. B* **83**, 235124 (2011).

- (2011). doi: <https://doi.org/10.1103/PhysRevB.83.235124>; O. El Araby, V. Gritsev, and A. Faribault, Bethe ansatz and ordinary differential equation correspondence for degenerate Gaudin models. *Phys. Rev. B* **85**, 115130 (2012). doi: <https://doi.org/10.1103/PhysRevB.85.115130>
- [42] X. Guan, K. D. Launey, M. X. Xie et al., Numerical algorithm for the standard pairing problem based on the Heine-Stieltjes correspondence and the polynomial approach. *Comp. Phys. Commun.* **185**, 2714 (2014). doi: <https://doi.org/10.1016/j.cpc.2014.05.023>
- [43] C. Qi, and T. Chen, Exact solution of the pairing problem for spherical and deformed systems. *Phys. Rev. C* **92**, 051304(R) (2015). doi: [10.1103/PhysRevC.92.051304](https://doi.org/10.1103/PhysRevC.92.051304)
- [44] X. Guan, H. C. Xu, F. Pan et al., Ground state phase transition in the Nilsson mean-field plus standard pairing model. *Phys. Rev. C* **94**, 024309 (2016). doi: <https://doi.org/10.1103/PhysRevC.94.024309>
- [45] X. Guan and C. Qi, An iterative approach for the exact solution of the pairing Hamiltonian. *Comp. Phys. Comm.* **275**, 108310 (2022). doi: <https://doi.org/10.1016/j.cpc.2022.108310>
- [46] X. Guan, Y. Xin, Y. J. Chen et al., Impact of pairing interactions on fission in the deformed mean-field plus standard pairing model. *Phys. Rev. C* **104**, 044329 (2021). doi: <https://doi.org/10.1103/PhysRevC.104.044329>
- [47] X. Guan, T. C. Wang, W. Q. Jiang et al., Impact of the pairing interaction on fission of U isotopes. *Phys. Rev. C* **107**, 034307 (2023). doi: <https://doi.org/10.1103/PhysRevC.107.034307>
- [48] X. Guan, J. H. Zheng, and M. Y. Zheng, Pairing effects on the fragment mass distribution of Th, U, Pu, and Cm isotopes. *Nucl. Sci. Tech.* **34**, 173 (2023). doi: [10.1007/s41365-023-01316-x](https://doi.org/10.1007/s41365-023-01316-x)
- [49] C. Schmitt, K. Pomorski, B. K. Nerlo-Pomorska et al., Performance of the Fourier shape parametrization for the fission process. *Phys. Rev. C* **95**, 034612 (2017). doi: [10.1103/PhysRevC.95.034612](https://doi.org/10.1103/PhysRevC.95.034612)
- [50] K. Pomorski, J. M. Blanco, P. V. Kostyukov et al., Fission fragment mass yields of Th to Rf even-even nuclei. *Chin. Phys. C* **45**, 054109 (2021). doi: [10.1088/1674-1137/abec69](https://doi.org/10.1088/1674-1137/abec69)
- [51] L. L. Liu, Y. J. Chen, X. Z. Wu et al., Analysis of nuclear fission properties with the Langevin approach in Fourier shape parametrization. *Phys. Rev. C* **103**, 044601 (2021). doi: [10.1103/PhysRevC.103.044601](https://doi.org/10.1103/PhysRevC.103.044601)
- [52] A. Bohr, The coupling of nuclear surface oscillations to the motion of individual nucleons. *Dan. Mat. Fys. Medd.* **26**, 14 (1952).
- [53] T. Kaniowska, A. Sobiczewski, K. Pomorski et al., Microscopic inertial functions for nuclei in the barium region. *Nucl. Phys. A* **274**, 151 (1976). doi: [https://doi.org/10.1016/0375-9474\(76\)90233-5](https://doi.org/10.1016/0375-9474(76)90233-5)
- [54] S. G. Rohoziński, and A. Sobiczewski, Hexadecapole Nuclear Potential for Non-Axial Shapes, *Acta Phys. Pol. B* **12**, 1001 (1981). doi: [10.1016/0003-4916\(82\)90273-1](https://doi.org/10.1016/0003-4916(82)90273-1)
- [55] P. Möller, A. J. Sierk, R. Bengtsson et al., *Atom. Data Nucl. Data Tables* **98**, 149 (2012). doi: [10.1103/PhysRevC.79.064304](https://doi.org/10.1103/PhysRevC.79.064304)
- [56] K. Pomorski, and J. Dudek, Nuclear liquid-drop model and surface-curvature effects. *Phys. Rev. C* **67**, 044316 (2003). doi: [10.1103/PhysRevC.67.044316](https://doi.org/10.1103/PhysRevC.67.044316)
- [57] V. M. Strutinsky, Shell effects in nuclear masses and deformation energies. *Nucl. Phys. A* **95**, 420 (1967). doi: [10.1016/0375-9474\(67\)90510-6](https://doi.org/10.1016/0375-9474(67)90510-6)
- [58] V. M. Strutinsky, 'Shells' in deformed nuclei. *Nucl. Phys. A* **122**, 1 (1968). doi: [10.1016/0375-9474\(68\)90699-4](https://doi.org/10.1016/0375-9474(68)90699-4)
- [59] S. G. Nilsson, C. F. Tsang, A. Sobiczewski, et al. On the nuclear structure and stability of heavy and superheavy elements. *Nucl. Phys. A* **95**, 1 (1969). doi: [10.1016/0375-9474\(69\)90809-4](https://doi.org/10.1016/0375-9474(69)90809-4)
- [60] Y. Sun, Projection techniques to approach the nuclear many-body problem. *Phys. Scr.* **91**, 043005 (2016). doi: [10.1088/0031-8949/91/4/043005](https://doi.org/10.1088/0031-8949/91/4/043005)
- [61] M. Bender, K. Rutz, P. G. Reinhard et al., Pairing gaps from nuclear mean-field models. *Eur. Phys. J. A* **8**, 59 (2000). doi: [10.1007/s10050-000-4504-z](https://doi.org/10.1007/s10050-000-4504-z)
- [62] U. S. National Nuclear Data Center: <http://www.nndc.bnl.gov/>